Equivalent polynomials for quadrature in Heaviside function enriched elements

G.Ventura*[1], E. Benvenuti[2]

[1] *Politecnico di Torino, Corso Duca degli Abruzzi 24, 10129 Torino, Italy*

[2] *University of Ferrara, Via Saragat 1, 44122 Ferrara, Italy*

SUMMARY

One of the advantages of local Partition of Unity finite element methods, like the eXtended Finite Element Method, is the ability of modeling discontinuities independent of the mesh structure. The enrichment of the element functional space with discontinuous or non-differentiable functions requires, when the element stiffness is computed, partitioning into subdomains for quadrature. However, the arbitrary intersection between the base mesh and the discontinuity plane generates quadrature subdomains of complex shape. This is particularly true in three-dimensional problems, where quite sophisticate methodologies have been presented in the literature for the element stiffness evaluation.

The present work addresses the problem of Heaviside function enrichments and is based on the replacement of the discontinuous enrichment function with an equivalent polynomial defined on the entire element domain. This allows for the use of standard Gaussian quadrature in the elements crossed by the discontinuity. The work is an extension of the first version of the equivalent polynomial methodology introduced in 2006. It allows to compute equivalent polynomials for all continuum element families in one, two and three dimensions. An error analysis for enriched elements with the literature and the proposed method is shown. Finally, an extension of the technique is presented, and equivalent polynomials are introduced in the case of non-polynomial stiffness terms. This is applied to the case of distorted quadrilateral elements, obtaining results much more accurate than traditional Gauss quadrature. Copyright © 2014 John Wiley & Sons, Ltd.

Received . . .

Copyright © 2014 John Wiley & Sons, Ltd.

Prepared using nmeauth.cls
DOI: 10.1002/nme

Int. J. Numer. Meth. Engng 2014; **00**:2–36
KEY WORDS: Quadrature, extended Finite Element Method, Generalized Finite Element Method, Heaviside Function, Enrichment, Level Sets.
Published online in Wiley InterScience (www.interscience.wiley.com). DOI: 10.1002/nme

1. INTRODUCTION

The development and application of of Partition of Unity Methods [1] has almost two decades, where many aspects have been developed with success as recalled by the reviews [2, 3, 4, 5]. The flexibility and performance of the methods derived by the Partition of Unity approach, like XFEM [4] and GFEM [6, 7] have produced a growing interest in the scientific community, proved by a significant increasingly trend in the number of papers published on this topic.

The peculiarity of these methods is well-known and is based on the enrichment of the representation space of finite elements with functions having features to be represented, e.g. discontinuities, singularities, jumps and so on. This allows to represent these features independently of the mesh structure and alignment and to obtain increased convergence rates.

However, the enrichment of the finite element space with singular or discontinuous functions brings the necessity of evaluating non-polynomial integrands when computing the stiffness matrix of the enriched element.

This aspect was not discussed by the early literature on XFEM and GFEM, in the sense that the problem was solved by partitioning the enriched elements at discontinuities and then applying standard quadrature rules. This was accomplished by introducing a sort of local remeshing at the element level to generate standard quadrature subcells where continuous and differentiable integrands were present.

Studies on convergence rates soon demonstrated that the very high potential of the method was significantly affected by the quadrature technique used for computing the stiffness matrix of the enriched elements. In between the first works highlighting explicitly this aspect we may recall [8], where the problem of the quadrature for dislocation problems was solved with a highly expensive

*Correspondence to: Giulio Ventura, Politecnico di Torino - DISEG, Corso Duca degli Abruzzi 24, 10129 Torino, Italy.
Email: giulio.ventura@polito.it

Copyright © 2014 John Wiley & Sons, Ltd.

adaptive technique based on the software library CUBPACK [9] and [10], where a new quadrature rule was proposed for crack tip fields.

The first literature papers explicitly devoted to this problem and having the word ”quadrature” in their title are, in chronological order [11], where the concept of equivalent polynomials was introduced and [12], where the relation between quadrature rules and the accuracy of XFEM crack tip fields was studied. As will be detailed in the following, the paper [11] is the basis of the present work.

Quadrature literature can be divided into two main groups: one is focused on crack tip fields and the other on displacement jumps. Jumps are typical of crack faces separation and are usually modeled by Heaviside function enrichment. In a crack propagation problem the Heaviside function enrichment is applied to a very large number of elements, so that an efficient implementation of this part is important.

It is useful to recall briefly the literature on quadrature techniques applied to XFEM. This excursus will be based on the employed techniques and will not follow the temporal development of the techniques.

A class of methods is based on conformal mappings [13, 14]. These methods are based on the consideration that an element cut by a discontinuity generates two non-standard integration domains (e.g. polygonal), where standard integration rules cannot be applied. Then, it is proposed to map the non-standard domains to a standard domain and then use known integration rules [15]. This is accomplished by Schwarz-Christoffel mapping of the polygonal domain to the unit disk, but its applicability is limited to two dimensional problems.

Specifically related to crack tip fields are the techniques based on singularity elimination. The first work based on this approach is [10]. Here the Authors observe that crack tip enrichments have a $r^{-\frac{1}{2}}$ singularity requiring quadrature rules with a very high number of integration points. Therefore, they propose to introduce a quadrature cell transformation eliminating the singularity. This allowed to obtain a drastic reduction of quadrature points although some limitations were still present like the fact that the crack tip must coincide with a vertex of the transformed quadrature

Copyright © 2014 John Wiley & Sons, Ltd.

Prepared using nmeauth.cls
DOI: 10.1002/nme

cell and the problem of a not immediate extension to three dimensions. However, this idea was an important cornerstone in XFEM quadrature of crack tip fields. The same path of reasoning was followed in [16], where the Authors map triangular/tetrahedral integration cells on the square/cube by a generalized Duffy transformation. This methodology has some important advantages: (a) singularities of the kind p/r^{α} can be dealt with, where p is a trivariate polynomial and $\alpha > 0$ is the strength of the singularity; (b) the method is applicable in 3D; (c) its coupling with a node elimination algorithm yields increased efficiency. A third mapping method was introduced in [17], where a generalization of Nagarajan and Mukherjee mapping [18] to three dimensions for crack problems was introduced. This transformation allows, like the previously cited, to eliminate the crack singularity in the integration process, enhancing its efficiency.

Another class of methods is devoted to the integration on polygonal domains. Here the problem under study is the fact that an element cut by a discontinuity generates polygonal subdomains, where standard integration rules cannot be applied. A solution is to compute the exact integration of monomials on the domain and generate a quadrature rule by solving the moment fitting equations, fixing a priori the location of the quadrature points and computing the relevant weights. Two main approaches have been used. The first is based on Lasserre's technique [19, 20, 21, 22], where the integration of homogeneous functions on convex polygons or polyhedra is transformed into line integrations over edges. The second is based on applications of the divergence theorem [23, 24, 25]. Although compared to Lasserre's technique it is formally more complex to apply, it does not have restrictions on the convexity of the domain or on the homogeneity of the integrand.

Some comparisons between different integration schemes have been recently given in [26].

Equivalent polynomials are in between the first studies dedicated to the quadrature in enriched elements [11]. This technique has been presented with reference to generalized Heaviside enrichments (used to represent jumps in the displacement field), although it can be applied to more general cases. For example, in [27] it has been used for regularized Heaviside functions.

The technique is based on the idea of replacing, in the evaluation of the stiffness matrix, the discontinuous Heaviside enrichment function with an equivalent polynomial. The equivalent

Copyright © 2014 John Wiley & Sons, Ltd.

Prepared using nmeauth.cls
DOI: 10.1002/nme

polynomial is defined in such a way the evaluated stiffness matrix is exact, without introducing any approximation. It allows for standard Gauss quadrature in the element, eliminating the need of domain partition for quadrature.

A closely and interesting related approach has been presented in [28], where quadrature rules for triangles and tetrahedra are found with weights depending on the position of the discontinuity in the element. This work, although following a different reasoning path, is related to equivalent polynomials in the sense that the computed weights will coincide with the values of the equivalent polynomial at Gauss points by definition.

This paper follows and expands conceptually the first work published in [11], overcoming some difficulties of the method and getting a deeper insight on its potential.

In particular, while both [11] and [28] were successful in obtaining the result for linear triangles and tetrahedra and for the bilinear rectangle in [11], solutions for hexahedra and higher order elements could not be found. This was a severe practical limitation in the application of equivalent polynomials. This limitation emanates from the fact that the methodology requires the computation of the exact solution for a generic position of the discontinuity to derive the polynomial coefficients. This task was easy for triangles and tetrahedra, more complex for rectangular elements (where the divergence theorem was used), and had no success for hexahedra due to the complexity of the potential intersections with the discontinuity plane, leading to huge mathematical expressions.

The present paper overcomes these difficulties and illustrates a new technique that allows for the computation of equivalent polynomials in hexahedra and higher order elements. Therefore, it allows to use systematically equivalent polynomials in Heaviside function enriched elements of any dimensionality and order.

The idea behind the new approach originates in [27, 29]. These works, dealing with imperfect interfaces, were employing a regularized Heaviside function to model the discontinuity. The introduction of a regularized Heaviside function brings noticeable problems in numerical quadrature as, depending on the value of the regularization parameter, very high gradients are generated. An accurate evaluation of these integrals was requiring very expensive adaptive quadratures, solved in

Copyright © 2014 John Wiley & Sons, Ltd.

Prepared using nmeauth.cls
DOI: 10.1002/nme

[27, 29] by the use of the package CUBPACK [9] and an application of equivalent polynomials that was yielding, however, quite complex final expressions.

Moving from these ideas, a new method is being presented in this paper. The method introduces the regularized Heaviside function not to smear the discontinuity, but for allowing analytic quadrature, finding the equivalent polynomials and then computing the derived expression in their limit to the exact, discontinuous Heaviside function. The derived expressions for the equivalent polynomials can be therefore used both for dealing with perfect and imperfect interfaces. A deep conceptual difference of this method with any other presented previously in the literature is that it never requires the evaluation of quantities connected somehow (with domain or surface/line integrations) to the two subdomains generated by the discontinuity surface: integration of the regularized Heaviside function is performed always on the entire element parent domain.

As evidenced in [11], the computation of equivalent polynomials in the element parent domain makes the technique exact for constant Jacobian elements (linear, triangular, tetrahedral) and approximate for elements with non-constant Jacobian like distorted quadrilaterals (with non parallel edges), where rational functions appear in the evaluation of the element stiffness.

The error analysis outlined in [11] is here significantly expanded. A different and more physical error measure, based on the eigenvalues of the stiffness matrix, is considered. A technique is introduced for significantly reduce the errors generated by the rational Jacobian and the equivalent polynomial mapping. This new technique, based on the use of higher order equivalent polynomials, opens new perspectives for all non-polynomial integrands and outperforms, in terms of accuracy of the evaluated stiffness, the classical quadrature on subcells.

The paper outline is as follows. Section 2 gives a brief recall of the Heaviside function enrichment in XFEM/GFEM and the concept of equivalent polynomial as introduced in [11]. The properties of equivalent polynomials are shown and the general structure for their determination is given. Section 3 introduces the new method based on the use of a regularized heaviside function. Results are given for illustration in the cases of the linear tetrahedron and hexahedron. A vector formulation is illustrated for improved numerical efficiency. Finally, Section 4 studies the error generated by

Copyright © 2014 John Wiley & Sons, Ltd.

Prepared using nmeauth.cls
DOI: 10.1002/nme

isoparametric mapping and introduces the concept of higher degree equivalent polynomial reporting the advantages in terms of accuracy in the determination of the element stiffness eigenvalues.

2. XFEM FORMULATION AND QUADRATURE WITH EQUIVALENT POLYNOMIALS.

The classical approximation to the displacement field in XFEM formulations is given by the well-known expression [4, 2]

$$\mathbf{u}(\mathbf{x}) = \sum_{I \in \mathcal{N}} N_I(\mathbf{x}) \left(\mathbf{u}_I + \mathbf{a}_I f_{\mathrm{e}}(\mathbf{x}) \right) \tag{1}$$

where $\mathbf{u}$ is the displacement field, $\mathcal{N}$ are the nodes of the finite element mesh, $N_I(\mathbf{x})$ the finite element shape functions, f_{e} the enrichment function, $\mathbf{u}_I$ and $\mathbf{a}_I$ the standard and enrichment nodal variables, respectively.

In the present work the enrichment function will be assumed given by the generalized Heaviside step function, Fig. 1

$$f_{\mathrm{e}}(\mathbf{x}) = H(\mathbf{x}) = \mathrm{sign}\left(d(\mathbf{x})\right) = \begin{cases} 1 & \text{if} \quad d(\mathbf{x}) > 0 \\ -1 & \text{if} \quad d(\mathbf{x}) < 0 \end{cases} \tag{2}$$

It is recalled that this function is quite useful in XFEM applications as it describes a displacement jump at $d = 0$, so it is of general use when dealing with cracks in any number of dimensions.

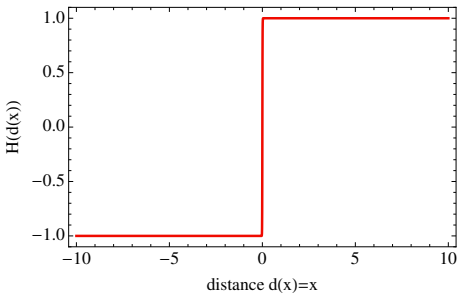

Figure 1. Enrichment function for crack problems.

The enrichment part in 1 is added only to the nodes of the elements cut by the discontinuity, so that these elements are called enriched elements.

Copyright © 2014 John Wiley & Sons, Ltd.

Prepared using nmeauth.cls
DOI: 10.1002/nme

The discontinuous function (2), enriching the finite element space by (1), will then enter the element stiffness matrix, so that Gaussian quadrature cannot be used unless the element domain is split into two subdomains, one for each side of the discontinuity. This can be immediately observed by applying the virtual work principle for determining the element stiffness: here the derivation presented in [11] is briefly recalled for introducing the notation used in this paper. Consider the restriction of the displacement and strain field in vector form to a single enriched finite element Ω_e

$$\mathbf{u} = \mathbf{N}\mathbf{u}_\mathrm{e} + H\mathbf{N}\mathbf{a}_\mathrm{e} \tag{3}$$

$$\boldsymbol{\varepsilon} = \mathbf{B}\mathbf{u}_\mathrm{e} + H\mathbf{B}\mathbf{a}_\mathrm{e} \tag{4}$$

where $\mathbf{u}_\mathrm{e}$, $\mathbf{a}_\mathrm{e}$ are the element standard and enriched nodal variables and $\nabla_{\boldsymbol{\varepsilon}}$ is the symmetric gradient operator, so that $\mathbf{B}\,\mathbf{u}_\mathrm{e} = (\nabla_{\boldsymbol{\varepsilon}}\mathbf{N})\ \mathbf{u}_\mathrm{e}$. In (4) the derivatives of H do not appear being zeroes.

Let $\mathbf{E}$ be the elastic operator, such that the stress $\boldsymbol{\sigma}$ is given by $\boldsymbol{\sigma} = \mathbf{E}\boldsymbol{\varepsilon}$. The element internal virtual work is given by

$$\begin{aligned} L_\mathrm{i} = \int_{\Omega_\mathrm{e}} \boldsymbol{\varepsilon}^\mathrm{T}\boldsymbol{\sigma}\,\mathrm{d}\Omega = \\ \int_{\Omega_\mathrm{e}} \mathbf{B}^\mathrm{T}\mathbf{E}\,\mathbf{B}\,\mathrm{d}\Omega\,\mathbf{u}_\mathrm{e}\cdot\mathbf{u}_\mathrm{e} + \int_{\Omega_\mathrm{e}} \left(H\mathbf{B}^\mathrm{T}\mathbf{E}\,\mathbf{B}\right)\,\mathrm{d}\Omega\,\mathbf{a}_\mathrm{e}\cdot\mathbf{u}_\mathrm{e} + \\ \int_{\Omega_\mathrm{e}} \left(H\mathbf{B}^\mathrm{T}\mathbf{E}\,\mathbf{B}\right)\,\mathrm{d}\Omega\,\mathbf{u}_\mathrm{e}\cdot\mathbf{a}_\mathrm{e} + \\ \int_{\Omega_\mathrm{e}} \left(H^2\mathbf{B}^\mathrm{T}\mathbf{E}\,\mathbf{B}\right)\,\mathrm{d}\Omega\,\mathbf{a}_\mathrm{e}\cdot\mathbf{a}_\mathrm{e} \end{aligned} \tag{5}$$

Consequently, considering that $H^2 = 1$, the element stiffness matrix is

$$\mathbf{K}_\mathrm{e} = \int_{\Omega_\mathrm{e}} \left[\begin{array}{c|c} \mathbf{B}^\mathrm{T}\mathbf{E}\,\mathbf{B} & H\mathbf{B}^\mathrm{T}\mathbf{E}\,\mathbf{B} \\ \hline H\mathbf{B}^\mathrm{T}\mathbf{E}\,\mathbf{B} & \mathbf{B}^\mathrm{T}\mathbf{E}\,\mathbf{B} \end{array}\right] \mathrm{d}\Omega \tag{6}$$

where the matrix has been partitioned into four submatrices according to the nodal variables $\mathbf{u}_\mathrm{e}$ and $\mathbf{a}_\mathrm{e}$. The stiffness matrix can be seen as the sum of a polynomial, Gauss integrable part, $\mathbf{K}_\mathrm{e}^{(\mathrm{p})}$ and a discontinuous part $\mathbf{K}_\mathrm{e}^{(\mathrm{d})}$ as follows

Copyright © 2014 John Wiley & Sons, Ltd.

Prepared using nmeauth.cls
DOI: 10.1002/nme

$$\mathbf{K}_{\mathrm{e}}^{(\mathrm{p})} = \int_{\Omega_{\mathrm{e}}} \left[\begin{array}{c|c} \mathbf{B}^{\mathrm{T}}\mathbf{E}\,\mathbf{B} & \mathbf{0} \\ \hline \mathbf{0} & \mathbf{B}^{\mathrm{T}}\mathbf{E}\,\mathbf{B} \end{array}\right] \mathrm{d}\Omega \tag{7}$$

$$\mathbf{K}_{\mathrm{e}}^{(\mathrm{d})} = \int_{\Omega_{\mathrm{e}}} \left[\begin{array}{c|c} \mathbf{0} & H\mathbf{B}^{\mathrm{T}}\mathbf{E}\,\mathbf{B} \\ \hline H\mathbf{B}^{\mathrm{T}}\mathbf{E}\,\mathbf{B} & \mathbf{0} \end{array}\right] \mathrm{d}\Omega \tag{8}$$

The integration of the discontinuous part $\mathbf{K}_{\mathrm{e}}^{(\mathrm{d})}$ is performed in the literature by splitting the integration domain into two parts Ω_{e}^1 and Ω_{e}^2 at the discontinuity, so that Gaussian quadrature can be applied on each subdomain. Alternatively, approaches based on the application of the Gauss-Green theorem to the two subdomains have been successfully used as well [23].

A procedure to recover the possibility of using Gaussian quadrature on the entire element domain has been suggested in [11]. It is based on introducing an equivalent polynomial function $\tilde{H}$ having the property that

$$\int_{\Omega_{\mathrm{e}}} \tilde{H}\mathbf{B}^{\mathrm{T}}\mathbf{E}\,\mathbf{B}\,\mathrm{d}\Omega = \int_{\Omega_{\mathrm{e}}^1} H\mathbf{B}^{\mathrm{T}}\mathbf{E}\,\mathbf{B}\,\mathrm{d}\Omega + \int_{\Omega_{\mathrm{e}}^2} H\mathbf{B}^{\mathrm{T}}\mathbf{E}\,\mathbf{B}\,\mathrm{d}\Omega \tag{9}$$

Once $\tilde{H}$ is determined it is

$$\mathbf{K}_{\mathrm{e}} = \int_{\Omega_{\mathrm{e}}} \left[\begin{array}{c|c} \mathbf{B}^{\mathrm{T}}\mathbf{E}\,\mathbf{B} & \tilde{H}\mathbf{B}^{\mathrm{T}}\mathbf{E}\,\mathbf{B} \\ \hline \tilde{H}\mathbf{B}^{\mathrm{T}}\mathbf{E}\,\mathbf{B} & \mathbf{B}^{\mathrm{T}}\mathbf{E}\,\mathbf{B} \end{array}\right] \mathrm{d}\Omega \tag{10}$$

Equation (10) is Gauss integrable, being each term polynomial. The derivation of $\tilde{H}$ for some finite elements has been carried out in [11]. Here it is recalled that, for (9) to hold, $\tilde{H}$ must be a polynomial whose degree is at least equal to the polynomial degree of the term $\mathbf{B}^{\mathrm{T}}\mathbf{E}\,\mathbf{B}$. As an example, for the linear triangular or tetrahedral element the term $\mathbf{B}^{\mathrm{T}}\mathbf{E}\,\mathbf{B}$ is constant, so the single Equation (9) suffices for the determination of $\tilde{H}$, which will be a constant depending on the location of the discontinuity. For the linear quadrilateral the shape functions are bilinear, so that the term

Copyright © 2014 John Wiley & Sons, Ltd.

Prepared using nmeauth.cls
DOI: 10.1002/nme

$\mathbf{B}^{\mathrm{T}}\mathbf{E}\,\mathbf{B}$ is quadratic. Then, as the polynomial coefficients multiplying $\tilde{H}$ vary depending on the element stiffness entry, the equivalence (9) is to hold for all power terms up to two, i.e.

$$\int_{\Omega_e} \tilde{H}\,\mathrm{d}\Omega = \int_{\Omega_e^1} H\,\mathrm{d}\Omega + \int_{\Omega_e^2} H\,\mathrm{d}\Omega \tag{11a}$$

$$\int_{\Omega_e} \tilde{H}\xi\,\mathrm{d}\Omega = \int_{\Omega_e^1} H\xi\,\mathrm{d}\Omega + \int_{\Omega_e^2} H\xi\,\mathrm{d}\Omega \tag{11b}$$

$$\int_{\Omega_e} \tilde{H}\eta\,\mathrm{d}\Omega = \int_{\Omega_e^1} H\eta\,\mathrm{d}\Omega + \int_{\Omega_e^2} H\eta\,\mathrm{d}\Omega \tag{11c}$$

$$\int_{\Omega_e} \tilde{H}\xi\eta\,\mathrm{d}\Omega = \int_{\Omega_e^1} H\xi\eta\,\mathrm{d}\Omega + \int_{\Omega_e^2} H\xi\eta\,\mathrm{d}\Omega \tag{11d}$$

$$\int_{\Omega_e} \tilde{H}\xi^2\,\mathrm{d}\Omega = \int_{\Omega_e^1} H\xi^2\,\mathrm{d}\Omega + \int_{\Omega_e^2} H\xi^2\,\mathrm{d}\Omega \tag{11e}$$

$$\int_{\Omega_e} \tilde{H}\eta^2\,\mathrm{d}\Omega = \int_{\Omega_e^1} H\eta^2\,\mathrm{d}\Omega + \int_{\Omega_e^2} H\eta^2\,\mathrm{d}\Omega \tag{11f}$$

where ξ and η are the element parent coordinates. Therefore, for Equations (11) to hold simultaneously, it is assumed

$$\tilde{H}(\xi,\eta) = c_0 + c_1\xi + c_2\eta + c_3\xi\eta + c_4\xi^2 + c_5\eta^2 \tag{12}$$

where the six constants $c_0 \ldots c_5$ are determined by solving the linear system (11).

This implies that, in general, the use of the equivalent polynomial function allows to apply standard Gaussian quadrature the cost of doubling the polynomial degree of the integrand in (10).

It is important to point out clearly that the equivalent polynomial $\tilde{H}$ is not an interpolation to the function H. The relation between an n degree equivalent polynomial and the original Heaviside function H for a fixed domain is given by the equivalence of the integrals of $\tilde{H}$ and H for every

Copyright © 2014 John Wiley & Sons, Ltd.

Prepared using nmeauth.cls
DOI: 10.1002/nme

monomial term up to the degree n. To fix the ideas we state the property and compute the equivalent polynomials in the one-dimensional case on the domain $\Omega = [0, 1]$. It must be

$$\int_\Omega \tilde{H}\,\mathrm{d}\Omega = \int_\Omega H\,\mathrm{d}\Omega \tag{13a}$$

$$\int_\Omega \tilde{H}x\,\mathrm{d}\Omega = \int_\Omega Hx\,\mathrm{d}\Omega \tag{13b}$$

$$\int_\Omega \tilde{H}x^2\,\mathrm{d}\Omega = \int_\Omega Hx^2\,\mathrm{d}\Omega \tag{13c}$$

$$\vdots \tag{13d}$$

$$\int_\Omega \tilde{H}x^n\,\mathrm{d}\Omega = \int_\Omega Hx^n\,\mathrm{d}\Omega \tag{13e}$$

Let $\delta \in \Omega$ the position of the discontinuity, so that $d(x) = x - \delta$. The following Figures 2, 3, 4 illustrate the plots of $\tilde{H}$ for the degrees $0...5$ at three positions of the discontinuity $\delta = 0.2,\ 0.5,\ 0.7$. It may be seen immediately that the graph of $\tilde{H}$ is visually unrelated to the graph of H, so that $\tilde{H}$ is not an interpolation to H. Note, finally, that the polynomial coefficients of $\tilde{H}$ are function of the position of the discontinuity. For example, the second degree equivalent polynomial for the one-dimensional case at hand is

$$\tilde{H} = 1 - 2\delta + \left(-2\delta^2 + 4\delta - 1\right)x + \left(-2\delta^3 + 3\delta^2 - \frac{1}{2}\right)x^2 \tag{14}$$

Equation (14) can be the basis for using, instead of equivalent polynomials, special variable weights Gauss quadrature rules according to the approach introduced by [28]. In this case the weights will be function of the position of the discontinuity and will be given by the values of the equivalent polynomial at the Gauss Points.

3. A NEW RESOLUTIVE APPROACH FOR COMPUTING EQUIVALENT POLYNOMIALS

The equivalence formulas (9) or (11) rely on the fact that, for solving the problem of the determination of the equivalent polynomial, the two integrals on Ω_e^1 and Ω_e^2 are to be evaluated

Copyright © 2014 John Wiley & Sons, Ltd.

Prepared using nmeauth.cls
DOI: 10.1002/nme

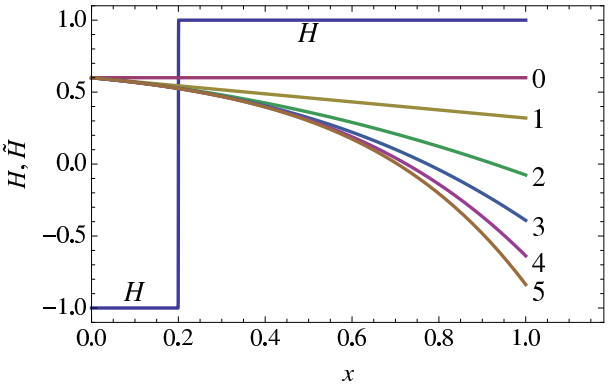

Figure 2. Graphs of H and the equivalent polynomials $\tilde{H}$ of degree $0...5$. The discontinuity is at $\delta = 0.2$. The number at the side of the curves is the degree of the equivalent polynomial.

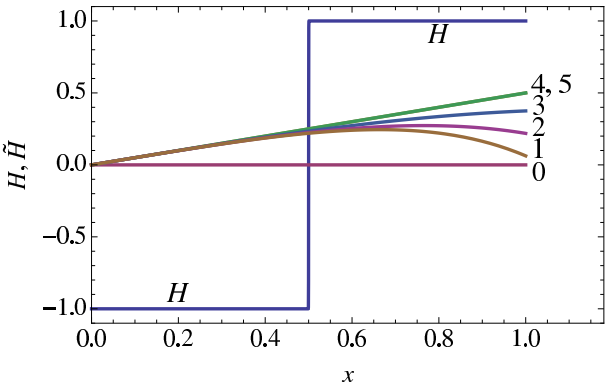

Figure 3. Graphs of H and the equivalent polynomials $\tilde{H}$ of degree $0...5$. The discontinuity is at $\delta = 0.5$. The number at the side of the curves is the degree of the equivalent polynomial.

analytically for a general position of the discontinuity. This was accomplished by different techniques (including the use of the divergence theorem) in [11]. Equivalent polynomials for some important cases were given, e.g. bar, linear triangle, linear tetrahedron, linear quadrilateral. But some cases, for example the linear hexahedron, could not be practically solved due to the geometric complexity of the integration subregions in which the element is subdivided by an arbitrary position of the discontinuity. This was a serious limitation to the equivalent polynomials approach.

A radically different approach to the problem has been then developed to eliminate the complexity stemming from the non-standard shape of the integration subdomains. This new approach relies on

Copyright © 2014 John Wiley & Sons, Ltd.

Prepared using nmeauth.cls
DOI: 10.1002/nme

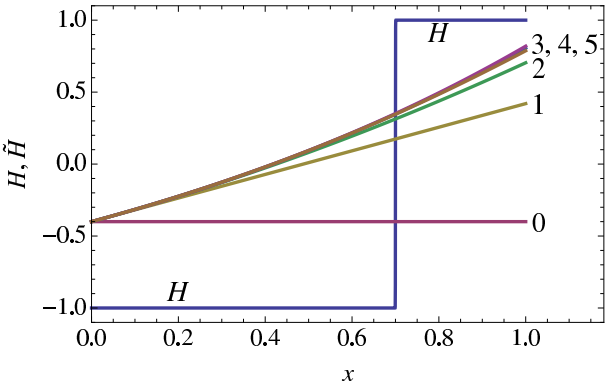

Figure 4. Graphs of H and the equivalent polynomials $\tilde{H}$ of degree $0...5$. The discontinuity is at $\delta = 0.7$. The number at the side of the curves is the degree of the equivalent polynomial.

the idea of replacing the Heaviside function with a regularized counterpart [27, 29], having the property of reverting to the original discontinuous function in the limit.

Consider the regularized form of the Heaviside function

$$H_\rho = \frac{2}{e^{-\rho x} + 1} - 1 \tag{15}$$

where e is the Euler's number and ρ is a regularization parameter. Some graphs of H_ρ are given in Figure 5. It can be observed that the discountinuous function H is reproduced as $\rho \to +\infty$. The motivation of introducing the regularized version of H is given by the fact that H_ρ is continuous and differentiable in $\mathbb{R}$ and its analytic primitive function is easily computed.

Therefore, the equivalent polynomial $\tilde{H}_\rho$ to H_ρ can be determined in closed form by the formal equivalence relation

$$\int_{\Omega_e} \tilde{H}_\rho \mathcal{M}^{(i)} \, \mathrm{d}\Omega = \int_{\Omega_e} H_\rho \mathcal{M}^{(i)} \, \mathrm{d}\Omega \qquad i = 1 \dots m \tag{16}$$

$\tilde{H}_\rho$ being the equivalent polynomial and $\mathcal{M}^{(i)}$ the monomial of degree i. Equations (16) are a system of m linear equations in the m unknown equivalent polynomial coefficients. Clearly, if n is the degree of the equivalent polynomial that it is to be computed, the number of monomials is

Copyright © 2014 John Wiley & Sons, Ltd.

Prepared using nmeauth.cls
DOI: 10.1002/nme

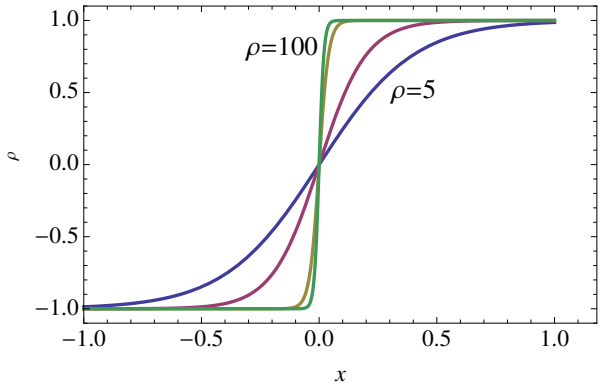

Figure 5. Graphs of H_ρ for increasing values of the regularization parameter ρ. As ρ diverges the regularized function graph reproduces the Heaviside function.

$m = (n+1)$ in one dimension, $m = (n+1)(n+2)/2$ in two dimensions and $m = (n+1)(n+2)(n+3)/6$ in three dimensions.

Taking the limit of (16) for $\rho \to +\infty$ it is

$$\lim_{\rho\to\infty} \int_{\Omega_e} \tilde{H}_\rho \mathcal{M}^{(i)} \, \mathrm{d}\Omega = \lim_{\rho\to\infty} \int_{\Omega_e} H_\rho \mathcal{M}^{(i)} \, \mathrm{d}\Omega \qquad i = 1 \dots m \tag{17}$$

and applying the bounded convergence theorem the limit and integration operators can be "swapped", so that

$$\int_{\Omega_e} \lim_{\rho\to\infty} \tilde{H}_\rho \mathcal{M}^{(i)} \, \mathrm{d}\Omega = \int_{\Omega_e} \lim_{\rho\to\infty} H_\rho \mathcal{M}^{(i)} \, \mathrm{d}\Omega \qquad i = 1 \dots m \tag{18}$$

Being

$$H\mathcal{M}^{(i)} = \lim_{\rho\to\infty} H_\rho \mathcal{M}^{(i)} \qquad i = 1 \dots m \tag{19}$$

it is, by definition of equivalent polynomial and (17), (18)

$$\tilde{H}\mathcal{M}^{(i)} = \lim_{\rho\to\infty} \tilde{H}_\rho \mathcal{M}^{(i)} \qquad i = 1 \dots m \tag{20}$$

and then

Copyright © 2014 John Wiley & Sons, Ltd.

Prepared using nmeauth.cls
DOI: 10.1002/nme

$$\tilde{H} = \lim_{\rho \to \infty} \tilde{H}_\rho \tag{21}$$

Therefore, the equivalent polynomial $\tilde{H}$ can be computed by taking the limit for $\rho \to \infty$ of $\tilde{H}_\rho$.

Consider, for the sake of illustration, the example one-dimensional case (13) introduced in the previous Section. Replacing H with H_ρ in (13) and solving, we obtain for the second degree equivalent polynomial the expression

$$\tilde{H}_\rho = \frac{x^2\left(12\rho\mathrm{Li}_2\left(-e^{-d\rho}\right)+12\rho\mathrm{Li}_2\left(-e^{\rho-d\rho}\right)+24\mathrm{Li}_3\left(-e^{-d\rho}\right)-24\mathrm{Li}_3\left(-e^{\rho-d\rho}\right)+\rho^3\right)}{2\rho^3}+$$
$$+\frac{x\left(-8\rho\mathrm{Li}_2\left(-e^{-d\rho}\right)+8\rho\mathrm{Li}_2\left(-e^{\rho-d\rho}\right)-8\rho^2\log\left(e^{(d-1)\rho}+1\right)+8\rho^2\log\left(e^{d\rho}+1\right)+8\rho^2\log\left(e^{\rho-d\rho}+1\right)-6\rho^3\right)}{2\rho^3}+$$
$$+\frac{4\rho^2\log\left(e^{(d-1)\rho}+1\right)-4\rho^2\log\left(e^{d\rho}+1\right)+2\rho^3}{2\rho^3}$$

where $\mathrm{Li}_n(f)$ is the polylogarithm function of order n and argument f, defined as:

$$\mathrm{Li}_n(f) = \sum_{k=1}^{\infty} \frac{f^k}{k^n} \tag{23}$$

whose evaluation is possible through numerical libraries.

It may be easily verified that the graph of (22) reproduces its limit polynomial for $\rho \to \infty$ (14) for even very low values of ρ, Figure 6.

3.1. Vector notation for improved numerical efficiency

The equivalence equations (16) are formed by a left hand side with a polynomial integrand that can be computed both in closed form or numerically, and a right hand side where the product of the regularized Heaviside function appear and that will be computed analytically. The equivalence is stated at the parent element level, so that the Jacobian related to the isoparametric mapping procedure does not appear. Its influence will be shown in Section 4. To get more compact results and improve efficiency it is advantageous to write the equivalence equations (16) in vector form [30]. Let

Copyright © 2014 John Wiley & Sons, Ltd.

Prepared using nmeauth.cls
DOI: 10.1002/nme

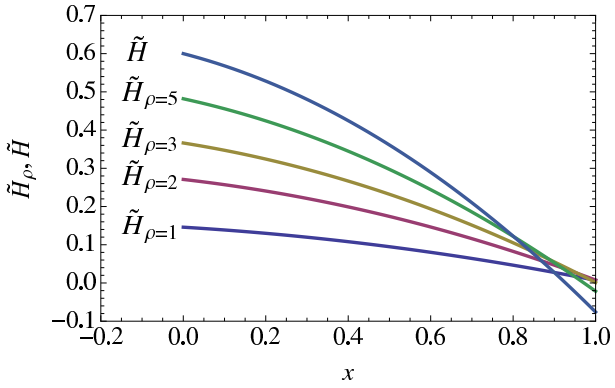

Figure 6. Graphs of the second degree equivalent polynomial $\tilde{H}_\rho$ for increasing values of the regularization parameter ρ and its limit function $\tilde{H}$.

$$\tilde{H}_\rho = \mathbf{C} \cdot \boldsymbol{\mathcal{M}} \tag{24}$$

where $\boldsymbol{\mathcal{M}}$ collects the monomials $\mathcal{M}^{(i)}$, $i = 1 \dots m$, the symbol $\cdot$ is the scalar product between vectors and $\mathbf{C}$ is the vector of the m unknown coefficients to be determined defining the equivalent polynomial. With this notation (16) is written

$$\int_{\Omega_e} \boldsymbol{\mathcal{M}}\boldsymbol{\mathcal{M}}^{\mathrm{T}} \,\mathrm{d}\Omega\, \mathbf{C} = \int_{\Omega_e} H_\rho \boldsymbol{\mathcal{M}} \,\mathrm{d}\Omega \tag{25}$$

Let

$$\mathbf{A} = \int_{\Omega_e} \boldsymbol{\mathcal{M}}\boldsymbol{\mathcal{M}}^{\mathrm{T}} \,\mathrm{d}\Omega \tag{26}$$

$$\mathbf{b} = \int_{\Omega_e} H_\rho \boldsymbol{\mathcal{M}} \,\mathrm{d}\Omega \tag{27}$$

From (25)(26) (27) the determination of the constants $\mathbf{C}$ is done by solving the linear system

$$\mathbf{AC} = \mathbf{b} \quad \Longrightarrow \quad \mathbf{C} = \mathbf{A}^{-1}\mathbf{b} \tag{28}$$

Copyright © 2014 John Wiley & Sons, Ltd.

Prepared using nmeauth.cls
DOI: 10.1002/nme

Note that $\mathbf{A}$ is a matrix of constants for each element family (e.g. linear tetrahedron, hexahedron, ...) and degree of the equivalent polynomial. Its evaluation is possible by Gaussian quadrature, $\mathbf{A}$ being given by products of monomials.

The difficulty in the application of the approach is therefore concentrated in the evaluation of the vector $\mathbf{b}$ given by (27).

As previously evidenced, the use of a regularized counterpart to the Heaviside function allows to carry the integration in (27) without partitioning the domain. It is however not convenient (although possible) to evaluate (27) numerically as this operation would be expensive considering the high gradients of H_ρ as ρ becomes large to reproduce the discontinuous Heaviside function H, Figure 5.

Therefore, the evaluation of $\mathbf{b}$ is done in closed form for an arbitrary position of the discontinuity and value of the regularization parameter ρ. Several continuous and differentiable approximations to H have been tried, and the selection of the form (15) has been done as it is integrable in closed form and produces the shortest results.

Concluding, $\mathbf{b}$ is evaluated Then, its analytic expression is evaluated numerically at each enriched element for a reasonably high value of ρ and the equivalent polynomial is computed by (28) and (24).

In the next Section results are given for the linear tetrahedron and hexahedron, but they can be derived for elements of any order and dimensionality.

3.2. Example: linear tetrahedron and hexahedron

The proposed approach for the computation of the equivalent polynomial by considering the regularized Heaviside function (15) is applied to the linear tetrahedron and hexahedron. In contrast to [11], here no intersection with the element edges and faces is explicitly needed, as the continuity and differentiability properties of (15) allow its integration in the entire parent element domain. Therefore, the discontinuity will be represented (or approximated) by a plane in the parent element domain, whose distance (level set) function p is given by

Copyright © 2014 John Wiley & Sons, Ltd.

Prepared using nmeauth.cls
DOI: 10.1002/nme

$$p(\xi,\eta,\zeta) = a\xi + b\eta + c\zeta + d \tag{29}$$

with a, b, c such that $\sqrt{a^2+b^2+c^2} = 1$. The value of p is the signed distance of a generic point at ξ, η, ζ from the discontinuity surface. Therefore, the regularized Heaviside function in this case will be simply given by

$$H_\rho = \frac{2}{e^{-\rho p(\xi,\eta,\zeta)}+1} - 1 \tag{30}$$

For the linear tetrahedron the equivalent polynomial is of degree zero (a constant), computed by solving the equivalence equation [11]

$$\int_{\Omega_e} \tilde{H}_\rho \,\mathrm{d}\Omega = \int_{\Omega_e} H_\rho \,\mathrm{d}\Omega \tag{31}$$

Due to the simplicity of this case the vector notation is not useful and the solution of (31) in the element parent domain $\Omega_e = \{\xi,\eta,\zeta \mid \xi\in[0,1], \eta\in[0,1], \zeta\in[0,1], \xi+\eta+\zeta \leqslant 1\}$ yields

$$\begin{aligned}\tilde{H}_\rho = \frac{1}{abc\rho^3(a-b)(a-c)(b-c)} \Big[& a\left(12c(a-c)\mathrm{Li}_3\left(-e^{(b+d)\rho}\right)+\right.\\ & -b(a-b)\left(c\rho^3(a-c)(b-c)+12\mathrm{Li}_3\left(-e^{(c+d)\rho}\right)\right)\Big)+\\ & +12(a-b)(a-c)(b-c)\mathrm{Li}_3\left(-e^{d\rho}\right)-12bc(b-c)\mathrm{Li}_3\left(-e^{(a+d)\rho}\right)\Big]\end{aligned} \tag{32a}$$

Equation (32) is apparently an indeterminate form for some values of the constants a, b, c defining the discontinuity plane. However, limits of the above quantities for all the needed cases (e.g. $a = b$, $a = c, \ldots$) can be analytically determined and implemented.

Similarly, for the linear hexahedron, due to the trilinearity of the shape functions the element stiffness contains the following monomials, that are assumed as terms of the equivalent polynomial

Copyright © 2014 John Wiley & Sons, Ltd.

Prepared using nmeauth.cls
DOI: 10.1002/nme

$$\boldsymbol{\mathcal{M}} = \big(1, \xi, \eta, \zeta, \xi^2, \eta^2, \zeta^2, \xi\eta, \xi\zeta, \eta\zeta, \tag{33}$$

$$\xi^2\eta, \xi^2\zeta, \eta^2\xi, \eta^2\zeta, \zeta^2\eta, \zeta^2\xi, \xi\eta\zeta, \tag{34}$$

$$\xi^2\eta\zeta, \eta^2\xi\zeta, \zeta^2\xi\eta, \xi^2\eta^2, \xi^2\zeta^2, \eta^2\zeta^2\big) \tag{35}$$

with the equivalence equations (16). In the element parent domain $\Omega_e = \{\xi, \eta, \zeta \mid \xi \in [-1,1], \eta \in [-1,1], \zeta \in [-1,1]\}$ the first four components of the vector $\mathbf{b}$ are reported in the following to show their analytic structure. Limits can be determined for the values of a, b, c that make the expressions indeterminate.

$$\begin{aligned} b_1 = -\frac{2}{abc\rho^3}\Big[&-\mathrm{Li}_3\left(-e^{-(a+b+c-d)\rho}\right) + \mathrm{Li}_3\left(-e^{(a-b-c+d)\rho}\right) + \mathrm{Li}_3\left(-e^{(-a+b-c+d)\rho}\right) + \\ &-\mathrm{Li}_3\left(-e^{(a+b-c+d)\rho}\right) + \mathrm{Li}_3\left(-e^{(-a-b+c+d)\rho}\right) - \mathrm{Li}_3\left(-e^{(a-b+c+d)\rho}\right) + \\ &-\mathrm{Li}_3\left(-e^{(-a+b+c+d)\rho}\right) + \mathrm{Li}_3\left(-e^{(a+b+c+d)\rho}\right) + 4abc\rho^3\Big] \end{aligned} \tag{36}$$

$$\begin{aligned} b_2 = -\frac{2}{a^2bc\rho^4}\Big[&a\rho\left(\mathrm{Li}_3\left(-e^{-(a+b+c-d)\rho}\right) + \mathrm{Li}_3\left(-e^{(a-b-c+d)\rho}\right) - \mathrm{Li}_3\left(-e^{(-a+b-c+d)\rho}\right) + \right. \\ &-\mathrm{Li}_3\left(-e^{(a+b-c+d)\rho}\right) - \mathrm{Li}_3\left(-e^{(-a-b+c+d)\rho}\right) - \mathrm{Li}_3\left(-e^{(a-b+c+d)\rho}\right) + \\ &\left.+\mathrm{Li}_3\left(-e^{(-a+b+c+d)\rho}\right) + \mathrm{Li}_3\left(-e^{(a+b+c+d)\rho}\right)\right) + \mathrm{Li}_4\left(-e^{-(a+b+c-d)\rho}\right) + \\ &-\mathrm{Li}_4\left(-e^{(a-b-c+d)\rho}\right) - \mathrm{Li}_4\left(-e^{(-a+b-c+d)\rho}\right) + \mathrm{Li}_4\left(-e^{(a+b-c+d)\rho}\right) + \\ &-\mathrm{Li}_4\left(-e^{(-a-b+c+d)\rho}\right) + \mathrm{Li}_4\left(-e^{(a-b+c+d)\rho}\right) + \\ &+\mathrm{Li}_4\left(-e^{(-a+b+c+d)\rho}\right) - \mathrm{Li}_4\left(-e^{(a+b+c+d)\rho}\right)\Big] \end{aligned} \tag{37}$$

Copyright © 2014 John Wiley & Sons, Ltd.

Prepared using nmeauth.cls
DOI: 10.1002/nme

$$b_3 = -\frac{2}{ab^2c\rho^4}\Big[b\rho\left(\mathrm{Li}_3\left(-e^{-(a+b+c-d)\rho}\right) - \mathrm{Li}_3\left(-e^{(a-b-c+d)\rho}\right) + \mathrm{Li}_3\left(-e^{(-a+b-c+d)\rho}\right) + \\ -\mathrm{Li}_3\left(-e^{(a+b-c+d)\rho}\right) - \mathrm{Li}_3\left(-e^{(-a-b+c+d)\rho}\right) + \mathrm{Li}_3\left(-e^{(a-b+c+d)\rho}\right) + \\ -\mathrm{Li}_3\left(-e^{(-a+b+c+d)\rho}\right) + \mathrm{Li}_3\left(-e^{(a+b+c+d)\rho}\right)\right) + \mathrm{Li}_4\left(-e^{-(a+b+c-d)\rho}\right) + \\ -\mathrm{Li}_4\left(-e^{(a-b-c+d)\rho}\right) - \mathrm{Li}_4\left(-e^{(-a+b-c+d)\rho}\right) + \mathrm{Li}_4\left(-e^{(a+b-c+d)\rho}\right) + \\ -\mathrm{Li}_4\left(-e^{(-a-b+c+d)\rho}\right) + \mathrm{Li}_4\left(-e^{(a-b+c+d)\rho}\right) + \mathrm{Li}_4\left(-e^{(-a+b+c+d)\rho}\right) + \\ -\mathrm{Li}_4\left(-e^{(a+b+c+d)\rho}\right)\Big] \tag{38}$$

$$b_4 = -\frac{2}{abc^2\rho^4}\Big[c\rho\left(\mathrm{Li}_3\left(-e^{-(a+b+c-d)\rho}\right) - \mathrm{Li}_3\left(-e^{(a-b-c+d)\rho}\right) - \mathrm{Li}_3\left(-e^{(-a+b-c+d)\rho}\right) + \\ +\mathrm{Li}_3\left(-e^{(a+b-c+d)\rho}\right) + \mathrm{Li}_3\left(-e^{(-a-b+c+d)\rho}\right) - \mathrm{Li}_3\left(-e^{(a-b+c+d)\rho}\right) + \\ -\mathrm{Li}_3\left(-e^{(-a+b+c+d)\rho}\right) + \mathrm{Li}_3\left(-e^{(a+b+c+d)\rho}\right)\right) + \mathrm{Li}_4\left(-e^{-(a+b+c-d)\rho}\right) - + \\ \mathrm{Li}_4\left(-e^{(a-b-c+d)\rho}\right) - \mathrm{Li}_4\left(-e^{(-a+b-c+d)\rho}\right) + \mathrm{Li}_4\left(-e^{(a+b-c+d)\rho}\right) + \\ -\mathrm{Li}_4\left(-e^{(-a-b+c+d)\rho}\right) + \mathrm{Li}_4\left(-e^{(a-b+c+d)\rho}\right) + \mathrm{Li}_4\left(-e^{(-a+b+c+d)\rho}\right) + \\ -\mathrm{Li}_4\left(-e^{(a+b+c+d)\rho}\right)\Big] \tag{39}$$

4. ISOPARAMETRIC MAPPING AND HIGHER ORDER EQUIVALENT POLYNOMIALS

In the present Section the effect of isoparametric mapping is considered and the concept of higher degree equivalent polynomial is introduced.

When an element is distorted and isoparametric mapping is used, sources of numerical error arise. These are connected with the fact that the integrand in the stiffness evaluation changes from a polynomial to a rational function and that the discontinuity is distorted by the mapping. These fundamental aspects of XFEM application are not investigated in the literature, but the associated approximation in the evaluation of the element stiffness is not negligible. This approximation may be acceptable in some problems (e.g. linear elastic fracture mechanics, where the edges of the crack are not loaded) but can be a source of error in some applications like cohesive cracks and hydraulic fracture.

Copyright © 2014 John Wiley & Sons, Ltd.

Prepared using nmeauth.cls
DOI: 10.1002/nme

In the present case an additional source of error may be present, originated by the fact that the equivalent polynomials are computed in the element parent domain, without accounting for the effect of the coordinate transformation.

A first study on this problem was presented in [11]. Then, it was realized that the way for measuring the error (the comparison of the values of the elements in the stiffness matrix) was not physically expressive and that some other aspects in the analysis should be further improved. Here that analysis is therefore briefly recalled, improved and expanded to get a much deeper insight on the problem and get a precise picture of its extent.

It has been pointed out that, in general, quadrature at the element level is performed in the parent domain by the well known isoparametric mapping, where the element global and parent reference frames are linked by a coordinate transformation.

In linear quadrilateral and hexahedral elements, when the opposite sides are non parallel, the inverse of the Jacobian is a rational function so that the integrand for the element stiffness evaluation is no longer polynomial. The traditional element Gaussian quadrature is therefore approximate and the proposed equivalent polynomial approach, exact for constant Jacobian, yields an approximate element stiffness matrix as well. Moreover, straight cracks are mapped to curved cracks in the parent element domain, introducing a new source of integration error even when element subdivision into quadrature subcells is used. Three sources of error are therefore into play

- element distortion
- discontinuity surface distortion
- approximate evaluation of the equivalent polynomial

These three aspects will be investigated in the following Section with reference to quadrilateral elements.

4.1. Distorted quadrilateral elements.

When computing the element stiffness for the quadrilateral element, a (2×2) Gauss point rule is usually chosen so to give exact quadrature in the parent domain. The fact that this quadrature rule is

Copyright © 2014 John Wiley & Sons, Ltd.

Prepared using nmeauth.cls
DOI: 10.1002/nme

not exact for distorted elements due to the non-constant determinant of the Jacobian and the rational function structure of the integrand is commonly accepted [31]. The order of magnitude of this error will be given in the following.

When enriching a distorted the element with the Heaviside function for representing a jump discontinuity, the shape of the discontinuity surface is altered by the isoparametric mapping. Two examples are given in Figs. 7 and 8, where it is shown how, when the element has non-parallel opposite sides, a straight discontinuity line in the element domain maps to a curve in the parent domain and vice-versa.

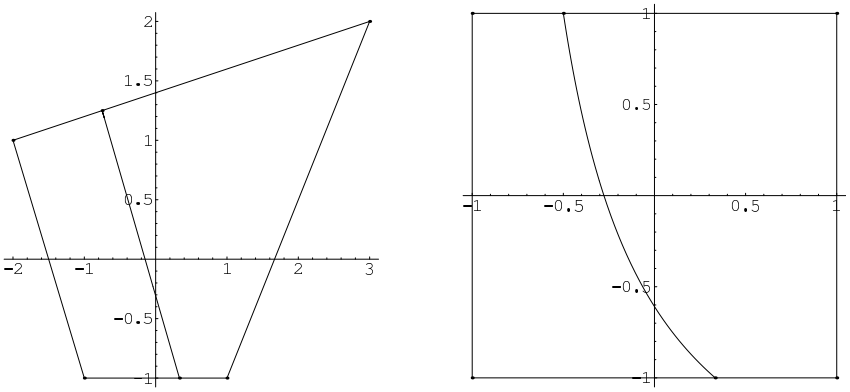

(a) (b)

Figure 7. Mapping of a line from a distorted element (a) to the parent domain (b).

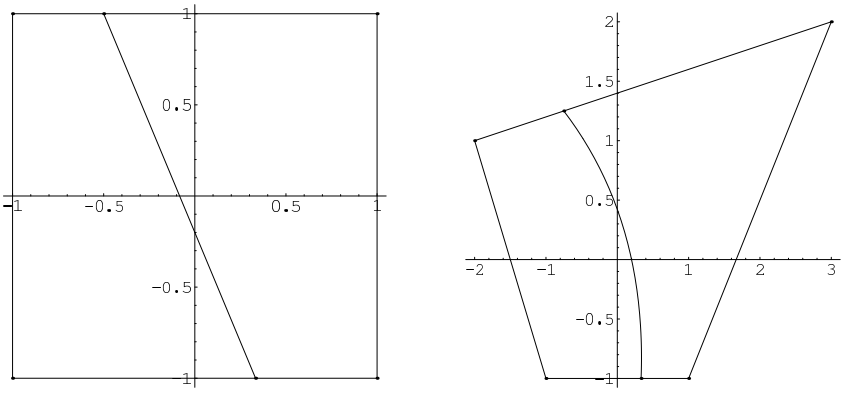

(a) (b)

Figure 8. Mapping of a line from the parent domain (a) to the distorted element domain (b).

Copyright © 2014 John Wiley & Sons, Ltd.

Prepared using nmeauth.cls
DOI: 10.1002/nme

As observed in [11], in the evaluation of the stiffness matrix by quadrature on subcells two approaches are therefore possible:

1. to assume a straight discontinuity line in the element domain and consider the two parts in which the element is split as quadrature subcells that will have then their own mappings for quadrature;
2. to assume a straight discontinuity line in the parent domain and define the two quadrature subcells in this reference.

Note that, if the first approach is used on a standard element (without enrichment), by arbitrarily splitting the element into two parts and then adding the stiffnesses computed in the two subcells, an error is observed as this sum will not be equal to the stiffness matrix computed on the entire element. This does not happen with the second approach where, if the contributions of the two quadrature subcells are added, the result coincides with the stiffness of the entire element.

Note that, in the use of equivalent polynomials, the second approach is adopted as the polynomial equivalence (16) is stated in the element parent domain. However, classical XFEM/GFEM literature employs the first approach.

Therefore two sources of error are present in every XFEM/GFEM implementation applied to distorted elements: the error generated by the rational integrand and the error generated by combining the rational integrand with the Heaviside function.

The element stiffness is formed by four sub matrices (6),(10). We will focus on the discontinuous part of the element stiffness (6) that is

$$\mathbf{K}_{\mathrm{e}(12)} = \int_{\Omega_{\mathrm{e}}} H\mathbf{B}^{\mathrm{T}}\mathbf{E}\,\mathbf{B}\mathrm{d}\Omega \tag{40}$$

To study the influence of the various factors pointed out, four cases of distorted quadrilateral elements are considered, and the stiffness matrix is computed in the following cases:

1. element without crossing discontinuity line (to look at the influence of the distortion only);
   (a) by adaptive numerical quadrature (exact value);

Copyright © 2014 John Wiley & Sons, Ltd.

Prepared using nmeauth.cls
DOI: 10.1002/nme

(b) by standard 2×2 Gauss quadrature;

2. element with crossing discontinuity;

   (a) by adaptive numerical quadrature (exact value);
   (b) by standard 2×2 Gauss quadrature applied to the two quadrature subcells in which the element is split;
   (c) by 3×3 Gauss quadrature introducing the equivalent polynomial $\tilde{H}$. The order of quadrature is increased as the use of equivalent polynomials doubles the degree of the integrand function [11].

While in Reference [11] the error in some of the above cases was computed as sup norm in between the elements of the stiffness matrix, with the consequence that the results may be misleading especially for the smallest values, here a different approach is considered. As the important factor is the strain energy stored inside the finite element, once the stiffness matrix is computed its eigenvalues are evaluated and a percentage error is given comparing the difference between the eigenvalues compared to the largest. More precisely, let λ_i^{exact} the eigenvalues of the stiffness matrix computed by adaptive quadrature sorted in descending order and $\lambda_i^{\text{approx}}$ the same eigenvalues computed by one of the above methods (fixed points Gauss rule or equivalent polynomial). The percentage error in the i-th eigenvalues is defined by

$$\mathcal{E}_i = 100 \frac{|\lambda_i^{\text{approx}} - \lambda_i^{\text{exact}}|}{\lambda_1^{\text{exact}}} \tag{41}$$

where it is to be noted that for any i the largest eigenvalue, λ_1^{exact}, always appears at the denominator.

For evaluating the errors introduced by the above sources we consider the three distorted quadrilaterals whose vertexes are listed in Table I and plotted in Fig.9. The two quadrilaterals are chosen one to have a strong non-parallelism between the opposite sides (Q1) and the other for being with a high elongation (Q2).

Copyright © 2014 John Wiley & Sons, Ltd.

Prepared using nmeauth.cls
DOI: 10.1002/nme

Table I. Distorted quadrilaterals considered for errors computation. The columns report the vertexes coordinates V1...V4.

Label	V1	V2	V3	V4
Q1	$(+1,-1)$	$(+3,+2)$	$(-2,+1)$	$(-1,-1)$
Q2	$(+3,-1)$	$(+6,+2)$	$(-5,+1)$	$(-3,-1)$

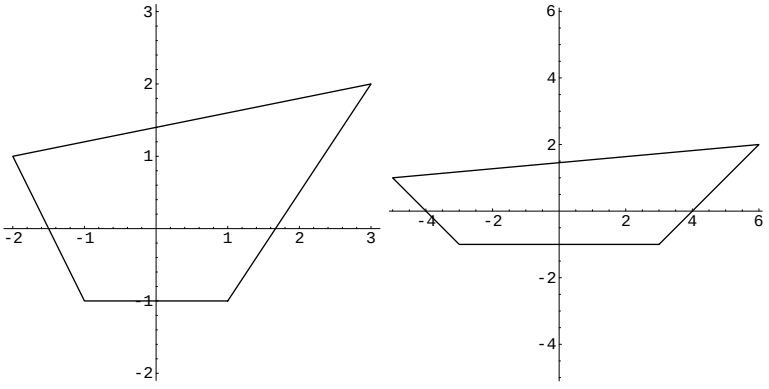

(a) (b)

Figure 9. Distorted quadrilaterals for error computations: (a) Q1; (b) Q2.

For the discontinuity inside the elements two cases are considered, labeled (a) and (b), respectively. In both cases the discontinuity line will cross two opposite element sides and it will have negative slope in case (a) and positive slope in case (b).

The intersection points $\mathbf{P}_1$ and $\mathbf{P}_2$ of the discontinuity in the parent coordinate system have coordinates $\mathbf{P}_1 = (4/5, -1)$, $\mathbf{P}_2 = (-3/4, +1)$ for case (a) and $\mathbf{P}_1 = (-4/5, -1)$, $\mathbf{P}_2 = (+3/4, +1)$ for case (b), Fig. 10. As previously pointed out, the discontinuity is assumed a line in the parent coordinate system, so that it is a curve in the physical domain.

Therefore, four situations will be considered, Q1(a), Q1(b), Q2(a) and Q2(b). The shape of the elements and the position of the discontinuity line have been chosen to be in between the worst error cases.

Table II lists the eigenvalues errors for the elements Q1 and Q2. No discontinuity is considered inside the elements and, as pointed out previously, the error arises from the 2×2 Gauss quadrature

Copyright © 2014 John Wiley & Sons, Ltd.

Prepared using nmeauth.cls
DOI: 10.1002/nme

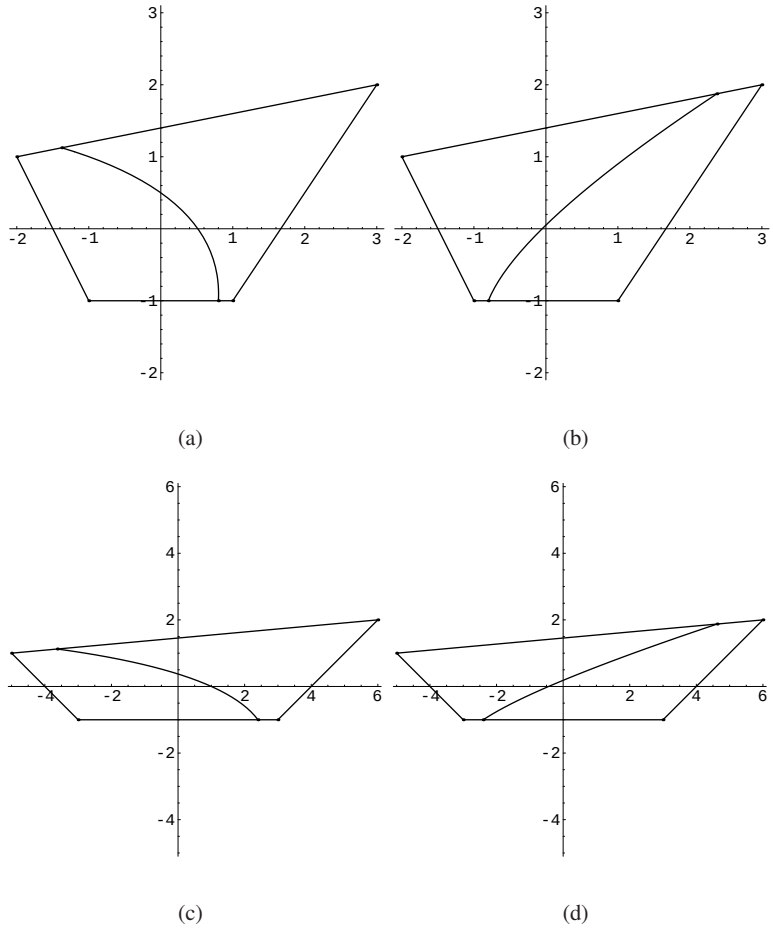

Figure 10. Distorted quadrilateral elements with discontinuity lines: (a) Case Q1(a), (b) Case Q1(b), (c) Case Q2(a), (d) Case Q2(b).

applied to the distorted elements, having rational stiffness integrand. The exact eigenvalues are computed by adaptive quadrature and it can be observed that the error is small and always less than 2%. Ideally, when the discontinuity line is introduced, the error should remain the same order of magnitude.

Now consider the two cases (a) and (b) of a discontinuity line and apply traditional subcells quadrature. The parent domain of the elements is subdivided into two quadrature subcells separated by the discontinuity line. Then 2×2 Gauss quadrature is applied to each subcells, while the exact stiffness is computed by adaptive quadrature. Tables III, IV reports the eigenvalues errors in the four examined cases Q1(a), Q1(b), Q2(a), Q2(b).

Copyright © 2014 John Wiley & Sons, Ltd.

Prepared using nmeauth.cls
DOI: 10.1002/nme

Table II. Errors in the stiffness eigenvalues due to element distortion and standard Gauss 2×2 quadrature rule. No discontinuity is considered.

Element	Eigenvalue	Percentage error $\mathcal{E}_i$
Q1	1	-0.13%
Q1	2	-0.29%
Q1	3	-1.27%
Q1	4	-0.80%
Q1	5	-1.18%
Q1	6	-0.05%
Q1	7	+0.00%
Q1	8	+0.00%
Q2	1	-0.04%
Q2	2	-0.14%
Q2	3	-0.37%
Q2	4	-0.84%
Q2	5	-0.07%
Q2	6	-0.00%
Q2	7	+0.00%
Q2	8	-0.00%

From Tables III, IV it can be seen that, in enriched distorted quadrilateral elements, the common practice of the quadrature on subcells introduces an error in the evaluation of the stiffness matrix that is commonly overlooked. The eigenvalue error can be the order of magnitude of 100%, i.e. much larger than that of non-enriched distorted elements.

The influence of the polynomial mapping is studied with the same technique. The equivalent polynomial $\tilde{H}$ is used for single cell quadrature in the evaluation of the stiffness matrix by (10). A

Copyright © 2014 John Wiley & Sons, Ltd.

Prepared using nmeauth.cls
DOI: 10.1002/nme

Table III. Errors in the stiffness eigenvalues due to element distortion and standard Gauss 2×2 quadrature rule on the two subcells generated by the discontinuity line.

Element	Discont. line	Eigenvalue	Percentage error $\mathcal{E}_i$
Q1	(a)	1	-0.35%
Q1	(a)	2	-1.07%
Q1	(a)	3	-93.9%
Q1	(a)	4	+87.3%
Q1	(a)	5	+0.03%
Q1	(a)	6	-0.19%
Q1	(a)	7	+0.00%
Q1	(a)	8	+0.00%
Q1	(b)	1	-1.21%
Q1	(b)	2	-0.73%
Q1	(b)	3	-1.94%
Q1	(b)	4	-1.83%
Q1	(b)	5	-0.11%
Q1	(b)	6	-0.09%
Q1	(b)	7	-0.00%
Q1	(b)	8	+0.00%

3×3 Gauss quadrature is used, being the degree of the polynomial integrand equal to 4. With these premises, Tables V, VI report the percentage eigenvalues errors for the examined cases.

From the results it appears quite evident that polynomial mapping has several advantages:

- the element is not split into quadrature subcells;
- the eigenvalues error is much inferior compared to quadrature on subcells: it decreases from a maximum of 94% (Table III) to a maximum of 3% (Table V). The order of magnitude of the error is therefore the same as traditional non-enriched distorted elements, see Table II.

Copyright © 2014 John Wiley & Sons, Ltd.

Prepared using nmeauth.cls
DOI: 10.1002/nme

Table IV. Errors in the stiffness eigenvalues due to element distortion and standard Gauss 2×2 quadrature rule on the two subcells generated by the discontinuity line.

Element	Discont. line	Eigenvalue	Percentage error $\mathcal{E}_i$
Q2	(a)	1	+0.91%
Q2	(a)	2	+0.36%
Q2	(a)	3	-77.8%
Q2	(a)	4	+77.0%
Q2	(a)	5	+0.03%
Q2	(a)	6	-0.00%
Q2	(a)	7	+0.00%
Q2	(a)	8	-0.00%
Q2	(b)	1	+0.32%
Q2	(b)	2	-0.05%
Q2	(b)	3	+0.57%
Q2	(b)	4	+0.29%
Q2	(b)	5	+0.01%
Q2	(b)	6	+0.01%
Q2	(b)	7	-0.00%
Q2	(b)	8	+0.00%

Note that this result contradicts apparently what reported in Reference [11] but, as pointed out before, the sup norm in between the elements of the stiffness matrix yields misleading results because of the differences in the vanishing elements of the matrix;

- the total number of Gauss points used in quadrature on subcells (2 subcells with 2×2 Gauss rule) and polynomial mapping (3×3 Gauss rule) is of the same order of magnitude, so no significant extra computational cost is involved.

Copyright © 2014 John Wiley & Sons, Ltd.

Prepared using nmeauth.cls
DOI: 10.1002/nme

Table V. Errors in the stiffness eigenvalues due to element distortion and polynomial mapping of the generalized Heaviside enrichment function.

Element	Discont. line	Eigenvalue	Percentage error $\mathcal{E}_i$
Q1	(a)	1	+1.24%
Q1	(a)	2	-0.08%
Q1	(a)	3	+2.88%
Q1	(a)	4	+1.29%
Q1	(a)	5	+0.22%
Q1	(a)	6	+0.07%
Q1	(a)	7	+0.00%
Q1	(a)	8	+0.00%
Q1	(b)	1	+2.50%
Q1	(b)	2	-1.52%
Q1	(b)	3	+1.53%
Q1	(b)	4	+1.20%
Q1	(b)	5	+0.31%
Q1	(b)	6	-0.28%
Q1	(b)	7	-0.00%
Q1	(b)	8	+0.00%

The results of the proposed polynomial mapping technique are therefore interesting. Moreover, it has been verified that they can be further improved by increasing the degree of the equivalent polynomial as described in the following.

To this end it is important to recall again the meaning of defining the equivalent polynomial. This concept is related in some way to polynomial interpolation: given a polynomial integrand of degree n times the enrichment function, the equivalent polynomial is defined by the property of having the same integral on the parent element domain as the original integrand. Because of the linearity of

Copyright © 2014 John Wiley & Sons, Ltd.

Prepared using nmeauth.cls
DOI: 10.1002/nme

Table VI. Errors in the stiffness eigenvalues due to element distortion and polynomial mapping of the generalized Heaviside enrichment function.

Element	Discont. line	Eigenvalue	Percentage error $\mathcal{E}_i$
Q2	(a)	1	-0.59%
Q2	(a)	2	-0.93%
Q2	(a)	3	+0.75%
Q2	(a)	4	+0.37%
Q2	(a)	5	-0.07%
Q2	(a)	6	-0.01%
Q2	(a)	7	+0.00%
Q2	(a)	8	-0.00%
Q2	(b)	1	+1.67%
Q2	(b)	2	+0.95%
Q2	(b)	3	-0.14%
Q2	(b)	4	-0.47%
Q2	(b)	5	+0.05%
Q2	(b)	6	-0.02%
Q2	(b)	7	-0.00%
Q2	(b)	8	+0.00%

the integral operator, this condition is equivalent to say that the equivalence property must hold for each monomial term. This yielded n conditions so an equivalent polynomial of degree n is naturally defined. To match the number of equations and unknowns the degree of the equivalent polynomial cannot be different from n: it basically interpolates the result.

The same path of reasoning can be applied to a non-polynomial integrand, like the one arising in distorted elements. In this case, the conceptual meaning of the system of equations defining the equivalent polynomial is different, as it will approximate (and not interpolate) the result. If we think

Copyright © 2014 John Wiley & Sons, Ltd.

Prepared using nmeauth.cls
DOI: 10.1002/nme

of the power expansion of the integrand, the equivalent polynomial realizes the exact integration of the terms of the expansion up to any chosen order n. Systems of equations of the kind (16) can be written up to any polynomial degree and the resulting equivalent polynomial gives an approximate solution to the quadrature problem. Note again that the equivalence equations are written always in the parent domain of the element, so that the Jacobian never enters the computation.

To verify the effectiveness of this approach consider the problem of the distorted quadrilaterals and the third degree equivalent polynomial

$$\tilde{H} = c_0 + c_1\,\xi + c_2\,\eta + c_3\,\xi\,\eta + c_4\,\xi^2 + c_5\,\eta^2 + c_6\,\xi\,\eta^2 + c_7\,\eta\,\xi^2 + c_8\,\xi^3 + c_9\,\eta^3 \qquad (42)$$

By writing and solving the equivalence equations up to third order the coefficients $c_0 \ldots c_9$ have been determined. Tables VII, VIII report the obtained results. Note that in this case the maximum polynomial degree of the integrand becomes 6, so that a 4×4 Gauss rule is required.

The results of Tables VII, VIII fully confirm the predicted result. In fact the eigenvalues error decreases to less than 0.2% and is therefore one order of magnitude less than the error of the simply distorted (non-enriched) element and three orders of magnitude less than quadrature on subcells.

This result non only demonstrates a further advantage of the polynomial mapping technique, but opens new perspectives for the reduction of quadrature errors in general finite element technology, whenever the stiffness matrix integrands are non-polynomial functions.

5. CONCLUSIONS.

The method of polynomial mapping, first introduced in [11], has been extended to elements of any order and dimensionality by introducing a regularized Heaviside function that is continuous, differentiable and integrable on the entire element domain. Then the result for the exact, discontinuous, Heaviside function is determined as a limit of the derived expressions. This eliminates completely any need for element partitioning into integration subcells or

Copyright © 2014 John Wiley & Sons, Ltd.

Prepared using nmeauth.cls
DOI: 10.1002/nme

Table VII. Errors in the stiffness eigenvalues due to element distortion and polynomial mapping of the generalized Heaviside enrichment function. Third degree equivalent polynomial.

Element	Discont. line	Eigenvalue	Percentage error $\mathcal{E}_i$
Q1	(a)	1	-0.19%
Q1	(a)	2	-0.01%
Q1	(a)	3	-0.16%
Q1	(a)	4	-0.02%
Q1	(a)	5	-0.03%
Q1	(a)	6	+0.01%
Q1	(a)	7	+0.00%
Q1	(a)	8	+0.00%
Q1	(b)	1	-0.07%
Q1	(b)	2	-0.01%
Q1	(b)	3	-0.10%
Q1	(b)	4	-0.03%
Q1	(b)	5	-0.03%
Q1	(b)	6	-0.01%
Q1	(b)	7	-0.00%
Q1	(b)	8	+0.00%

subsurfaces/edges. The method allows to compute the stiffness matrix of elements arbitrarily intersected by discontinuity planes of given equation in the parent reference. Moreover, the effect of element distortion and enrichment has been studied yielding interesting results on the accuracy of the stiffness eigenvalues and demonstrating the potential of equivalent polynomials for cases where non-polynomial functions are involved.

REFERENCES

Copyright © 2014 John Wiley & Sons, Ltd.

Prepared using nmeauth.cls
DOI: 10.1002/nme

Table VIII. Errors in the stiffness eigenvalues due to element distortion and polynomial mapping of the generalized Heaviside enrichment function. Third degree equivalent polynomial.

Element	Discont. line	Eigenvalue	Percentage error $\mathcal{E}_i$
Q2	(a)	1	-0.05%
Q2	(a)	2	+0.00%
Q2	(a)	3	-0.05%
Q2	(a)	4	+0.00%
Q2	(a)	5	+0.00%
Q2	(a)	6	+0.00%
Q2	(a)	7	+0.00%
Q2	(a)	8	-0.00%
Q2	(b)	1	+0.00%
Q2	(b)	2	+0.01%
Q2	(b)	3	+0.00%
Q2	(b)	4	+0.04%
Q2	(b)	5	+0.00%
Q2	(b)	6	+0.00%
Q2	(b)	7	-0.00%
Q2	(b)	8	+0.00%

1. Melenk J, Babuska I. The partition of unity finite element method: Basic theory and applications. *Computer Methods in Applied Mechanics and Engineering* 1996; **39**:289–314.
2. Fries TP, Belytschko T. The extended/generalized finite element method: An overview of the method and its applications. *International Journal for Numerical Methods in Engineering* 2010; **84**(3):253–304.
3. Yazid A, Abdelkader N, Abdelmadjid H. A state-of-the-art review of the x-fem for computational fracture mechanics. *Applied Mathematical Modelling* 2009; **33**(12):4269 – 4282.
4. Belytschko T, Gracie R, Ventura G. A review of extended/generalized finite element methods for material modeling. *Modelling and Simulation in Materials Science and Engineering* 2009; **17**(4):043 001.

Copyright © 2014 John Wiley & Sons, Ltd.

Prepared using nmeauth.cls
DOI: 10.1002/nme

5. Abdelaziz Y, Hamouine A. A survey of the extended finite element. *Computers and Structures* 2008; **86**(11-12):1141 – 1151.
6. Strouboulis T, Babuška I, Copps T. The design and analysis of the generalized finite element method. *Computer Methods in Applied Mechanics and Engineering* 2000; **181**:43–69.
7. Duarte C, Babuška I, Oden J. Generalized finite element method for three-dimensional structural mechanics problems. *Computers and Structures* 2000; **77**:219–232.
8. Ventura G, Moran B, Belytschko T. Dislocations by partition of unity. *Journal for Numerical Methods in Engineering* 2005; **62**:14631487.
9. Cools R, Laurie D, Pluym L. Cubpack++: A c++ package for automatic two-dimensional cubature. *ACM Trans. Math. Software* 1997; **23**:1–15.
10. Laborde P, Pommier J, Renard Y, Salaün M. High-order extended finite element method for cracked domains. *International Journal for Numerical Methods in Engineering* 2005; **64**(3):354–381.
11. Ventura G. On the elimination of quadrature subcells for discontinuous functions in the extended finite-element method. *International Journal for Numerical Methods in Engineering* 2006; **66**:761–795.
12. Xiao QZ, Karihaloo BL. Improving the accuracy of xfem crack tip fields using higher order quadrature and statically admissible stress recovery. *International Journal for Numerical Methods in Engineering* 2006; **66**(9):1378–1410.
13. Natarajan S, Bordas S, Roy Mahapatra D. Numerical integration over arbitrary polygonal domains based on schwarz-christoffel conformal mapping. *International Journal for Numerical Methods in Engineering* 2009; **80**(1):103–134.
14. Natarajan S, Mahapatra DR, Bordas SPA. Integrating strong and weak discontinuities without integration subcells and example applications in an xfem/gfem framework. *International Journal for Numerical Methods in Engineering* 2010; **83**(3):269–294.
15. Stroud A. *Approximate Calculation of Multiple Integrals*. Prentice Hall: Englewood Cliffs, N.J., 1971.
16. Mousavi S, Sukumar N. Generalized gaussian quadrature rules for discontinuities and crack singularities in the extended finite element method. *Computer Methods in Applied Mechanics and Engineering* 2010; **199**(49-52):3237 – 3249.
17. Park K, Pereira JP, Duarte CA, Paulino GH. Integration of singular enrichment functions in the generalized/extended finite element method for three-dimensional problems. *International Journal for Numerical Methods in Engineering* 2009; **78**(10):1220–1257.
18. Nagarajan A, Mukherjee S. A mapping method for numerical evaluation of two-dimensional integrals with 1/r singularity. *Computational Mechanics* 1993; **12**(1-2):19–26.
19. Lasserre J. Integration on a convex polytope. *Proceedings of the American Mathematical Society* 1998; **126**(8):2433–2441.
20. Lasserre J. Integration and homogeneous functions. *Proceedings of the American Mathematical Society* 1999; **127**(3):813–818.

Copyright © 2014 John Wiley & Sons, Ltd.

Prepared using nmeauth.cls
DOI: 10.1002/nme

21. Mousavi S, Sukumar N. Numerical integration of polynomials and discontinuous functions on irregular convex polygons and polyhedrons. *Computational Mechanics* 2011; **47**(5):535–554.
22. Kästner M, Müller S, Goldmann J, Spieler C, Brummund J, Ulbricht V. Higher-order extended fem for weak discontinuities - level set representation, quadrature and application to magneto-mechanical problems. *International Journal for Numerical Methods in Engineering* 2013; **93**(13):1403–1424.
23. Sudhakar Y, Wall WA. Quadrature schemes for arbitrary convex/concave volumes and integration of weak form in enriched partition of unity methods. *Computer Methods in Applied Mechanics and Engineering* 2013; **258**:39 – 54.
24. Müller B, Kummer F, Oberlack M. Highly accurate surface and volume integration on implicit domains by means of moment-fitting. *International Journal for Numerical Methods in Engineering* 2013; **96**(8):512–528.
25. Ventura G, Gracie R, Belytschko T. Fast integration and weight function blending in the extended finite element method. *International Journal for Numerical Methods in Engineering* 2009; **77**(1):1–29.
26. Abedian A, Parvizian J, Düster A, Khademyzadeh H, Rank E. Performance of different integration schemes in facing discontinuities in the finite cell method. *International Journal of Computational Methods* 2013; **10**(3):1350 002.
27. Benvenuti E, Tralli A, Ventura G. A regularized xfem model for the transition from continuous to discontinuous displacements. *International Journal for Numerical Methods in Engineering* 2008; **74**(6):911–944.
28. Holdych DJ, Noble DR, Secor RB. Quadrature rules for triangular and tetrahedral elements with generalized functions. *International Journal for Numerical Methods in Engineering* 2008; **73**(9):1310–1327.
29. Benvenuti E, Ventura G, Ponara N, Tralli A. Variationally consistent extended fe model for 3d planar and curved imperfect interfaces. *Computer Methods in Applied Mechanics and Engineering* 2013; **267**:434 – 457.
30. Esnault J. étude expérimental et numérique 3d du développement en fatigue d'une fissure déversée dans une tôle mince mtallique. PhD Thesis, Ecole Polytechnique, France 2014.
31. Bathe K. *Finite Element Procedures*. Prentice-Hall: Upper Saddle River, New Jersey, U.S.A., 1996.

Copyright © 2014 John Wiley & Sons, Ltd.

Prepared using nmeauth.cls
DOI: 10.1002/nme